Quantum correlations in spin chains

Artur Niezgoda⊙, Miłosz Panfil⊙, and Jan Chwedeńczuk⊙

Faculty of Physics, University of Warsaw, ul. Pasteura 5, PL-02-093 Warszawa, Poland

In this work, we address the question of how quantum is a collection of qubits, such as a chain of spins, a two-mode Bose-Einstein condensate, or a multiphoton state. We demonstrate that a single element of the density matrix carries the answer. Properly analyzed it brings information about the extent of the many-body entanglement and the nonlocality. This method can be used to tailor and witness highly nonclassical effects in many-body systems with possible applications to quantum computing, ultraprecise metrology, or large-scale tests of quantum mechanics. As a proof of principle, we investigate the extent of nonlocality and entanglement in ground states and thermal states of experimentally accessible interacting spin chains.

I. INTRODUCTION

An ensemble of qubits is a paradigm of a complex many-body quantum system—an ideal probe of various aspects of the theory, ranging from quantum phase transitions [1] to many-body entanglement [2] or the nonlocality [3]. Correlated states of many qubits are at the core of quantum-enhanced metrology [2,4], quantum-information processing [5], and tests of foundations of quantum mechanics. The quantum information aspects play an increasingly important role in condensed matter physics [6]. The experimental advances in the field of quantum simulators made it possible to prepare and control with great precision quantum many-body states [7]. The expanding toolbox includes ultracold atoms [8–15], trapped ions [16–22], and superconducting qubits [23–25] among others.

Given the growing interest it is relevant to adequately characterize the quantum features of a multiqubit state. What can we learn about it given a value of some correlation function? Is it quantum or can this correlation be reproduced with a classical ensemble? We address these questions in a systematic way relevant for experimentally realizable systems of dozens of qubits. Many powerful measures of entanglement, such as the entanglement entropy [6,26–32] or negativity [33–35], require detailed knowledge of the density matrix which makes their experimental measurements challenging [36,37]. In this work we propose an alternative approach. We show that a single element of the density matrix—related to the formation probability [38–41]—carries precise information about the many-body entanglement [42] and the ultraquantum Bell nonlocality [43–45].

The backbone of our work relies on a class of Bell inequalities, discussed in Sec. II, which make no assumption on the number of particles/subsystems or on how the local outcomes are bounded [46–48]. Our aim is in understanding the extent of entanglement and nonlocality in the multiqubit states, as explained in Sec. II, and for illustration in Sec. III we take the paradigmatic and experimentally accessible quantum Ising model [49–52], the *XXZ* spin chain [53,54], and the

Majumdar-Ghosh model [55,56]. For example, this method allows one to distinguish the situation in which the six-spin ground state of the Ising chain is actually a state where the entanglement and nonlocality extends over all spins (six-partite entanglement [57,58]), from a state in which quantum correlation encompasses only four spins. The experimental implementation of the devised protocol requires single-atom resolved detection which is within the range of experimental techniques [59,60]. Besides enriching our understanding of quantum correlated states of matter, such information should be useful in optimization of numerical approaches such as density matrix renormalization groups [61,62] and related methods [63,64]. Illustrated here with spin chains, this method can be applied to any multiqubit state, such as formed with Bose-Einstein condensates [65,66] or many-photon configurations [67,68]. We present the conclusions and the outlook in Sec. IV. Some details of the calculations leading to the results presented in the main text are contained in the Appendices.

II. THE BELL INEQUALITY FOR *N* QUBITS

We consider a system composed of N parts. Measurements of each yield two binary outcomes $\sigma_x^{(k)} = \pm 1$ and $\sigma_y^{(k)} = \pm 1$ (with $k = 1 \ldots N$). We introduce a correlator

$$\mathcal{C}_N = \langle \sigma^{(1)} \cdots \sigma^{(N)} \rangle, \tag{1}$$

where $\sigma^{(k)} = \frac{1}{2}(\sigma_x^{(k)} + i\sigma_y^{(k)})$. The "+" sign here can be changed to "−" independently for each party and the arguments that follow hold. If the above mean can be reproduced with a probability distribution $p(\lambda)$ of a random (hidden) variable λ, that correlates the outcomes in a classical way, i.e.,

$$\mathcal{C}_N = \int d\lambda \, p(\lambda) \sigma^{(1)}(\lambda) \cdots \sigma^{(N)}(\lambda), \tag{2}$$

then the correlator is consistent with a local hidden-variable (LHV) theory. Using a Cauchy-Schwarz inequality (CSI) we obtain the following Bell inequality [46,69] for $\mathcal{E}_N = |\mathcal{C}_N|^2$:

$$\mathcal{E}_N \leqslant \int d\lambda \, p(\lambda) |\sigma^{(1)}(\lambda)|^2 \cdots |\sigma^{(N)}(\lambda)|^2 = 2^{-N}, \tag{3}$$

where the last step is a consequence of $|\sigma^{(k)}(\lambda)|^2 = \frac{1}{2}$. If we consider quantum-mechanical systems, then $\sigma^{(k)}(\lambda)$'s are replaced by the Pauli rising operators for each qubit. The Bell inequality then reads

$$\mathcal{E}_N = \left| \left\langle \bigotimes_{k=1}^{N} \hat{\sigma}_+^{(k)} \right\rangle \right|^2 \leqslant 2^{-N}. \qquad (4)$$

The breaking of this inequality proves that qubits form a nonlocal state. The same correlator is also a witness of entanglement. For a separable state of N qubits, $\sigma^{(k)}(\lambda)$'s in (3) are replaced with $\langle \hat{\sigma}_+^{(k)} \rangle_\lambda \equiv \mathrm{Tr}[\hat{\varrho}^{(k)}(\lambda) \hat{\sigma}_+^{(k)}]$. Since $|\langle \hat{\sigma}_+^{(k)} \rangle|_\lambda^2 \leqslant \frac{1}{4}$, then

$$\mathcal{E}_N \leqslant \int d\lambda \, p(\lambda) \prod_{k=1}^{N} |\langle \hat{\sigma}_+^{(k)} \rangle|_\lambda^2 \leqslant 4^{-N} \qquad (5)$$

holds for all separable states [48]. To summarize, when $\mathcal{E}_N > 4^{-N}$, qubits are entangled. When $\mathcal{E}_N > 2^{-N}$, they are entangled and form a nonlocal state.

Note that, according to Eq. (4), $\mathcal{E}_N = |\varrho_{a,b}|^2$, where $\varrho_{a,b}$ is a component of the density matrix that couples $|\psi_a\rangle \equiv |\uparrow_1, \ldots, \uparrow_N\rangle$ with $|\psi_b\rangle \equiv |\downarrow_1, \ldots, \downarrow_N\rangle$, while

$$\hat{\sigma}_+^{(k)} |\downarrow_k\rangle = |\uparrow_k\rangle.$$

This is an important observation—the $\mathcal{E}_N$ extracts entanglement and nonlocality from a single element of the density matrix. Moreover, this leads to a size-independent upper bound

$$\mathcal{E}_N = |\varrho_{a,b}|^2 \leqslant \varrho_{a,a} \varrho_{b,b} \leqslant \frac{1}{4}, \qquad (6)$$

which implies that the inequality (5) can be violated starting already from $N = 2$, while the inequality (4) from $N = 3$. Both are saturated by the maximally entangled Greenberger-Horne-Zeilinger (GHZ) state

$$|\psi\rangle = \frac{1}{\sqrt{2}} (|\uparrow^{\otimes N}\rangle + |\downarrow^{\otimes N}\rangle). \qquad (7)$$

We now argue that the value of $\mathcal{E}_N$ carries detailed information on the multiparticle entanglement and nonlocality. We illustrate this with three density matrices of different character.

Many-body entanglement and nonlocality

In the first example we consider a system, where out of N qubits, two form an entangled state, and the other $N - 2$ are separable, i.e.,

$$\hat{\varrho}_N = \int d\lambda \, p(\lambda) \left(\bigotimes_{k=1}^{N-2} \hat{\varrho}^{(k)}(\lambda) \right) \otimes \hat{\varrho}_2(\lambda). \qquad (8)$$

[The lower index of the density matrix is the number of qubits it describes, while the upper index (k) labels a single kth qubit.] For this density matrix, the correlator $\mathcal{E}_N$ can be bounded using the CSI as follows:

$$\mathcal{E}_N \leqslant \int d\lambda \, p(\lambda) \mathcal{E}_{N-2}(\lambda) \int d\lambda \, p(\lambda) \mathcal{E}_2(\lambda) \leqslant 4^{-(N-1)}, \quad (9)$$

where $\mathcal{E}_{N-2}(\lambda)$ is calculated with the product state of $N - 2$ qubits, so $\mathcal{E}_{N-2}(\lambda) \leqslant 4^{-(N-2)}$, and $\mathcal{E}_2(\lambda)$ is the two-qubit

correlator calculated with the density matrix $\hat{\varrho}_2(\lambda)$, so $\mathcal{E}_2(\lambda) \leqslant 4^{-1}$. Inequality (9) is saturated by a product of a two-qubit GHZ state (7) and $N - 2$ states $|\psi_k\rangle = 1/\sqrt{2}(|\uparrow_k\rangle + e^{i\varphi_k}|\downarrow_k\rangle)$, where φ_k is an arbitrary phase. The violation of the bound (9), more stringent than (5), signals that the entanglement extends either over more pairs than just one or over more than a pair (three-qubit entanglement or more).

As a second example, we analyze the state with pairwise entangled qubits, which reads

$$\hat{\varrho}_N = \int d\lambda \, p(\lambda) \bigotimes_{k=1}^{N/2} \hat{\varrho}_2^{(k)}(\lambda), \qquad (10)$$

where $\hat{\varrho}_2^{(k)}(\lambda)$ is a density operator of the kth pair (we took N even for simplicity). In this case $\mathcal{E}_N \leqslant 4^{-N/2}$ and if violated, the state is at least three-qubit entangled.

Finally, if all but one qubit form an $N - 1$ entangled state, separable with the Nth qubit,

$$\hat{\varrho}_N = \int d\lambda \, p(\lambda) \hat{\varrho}_{N-1}(\lambda) \otimes \hat{\varrho}^{(N)}(\lambda), \qquad (11)$$

then $\mathcal{E}_N < \frac{1}{16}$. Values of the correlator from the range $]\frac{1}{16}, \frac{1}{4}]$ would imply then the N-particle entanglement.

Similarly, the value of $\mathcal{E}_N$ brings information about the extent of nonlocal correlations in the multiqubit system. For instance, when the correlation among no more than three out of N qubits cannot be explained with a LHV theory, then, in analogy to (9)

$$\mathcal{E}_N \leqslant \int d\lambda \, p(\lambda) \mathcal{E}_{N-3}(\lambda) \int d\lambda \, p(\lambda) \mathcal{E}_3(\lambda) \leqslant 2^{-(N-1)}. \quad (12)$$

Here we used the fact that for the locally correlated $N - 3$ qubits, $\mathcal{E}_{N-3}(\lambda) \leqslant 2^{-(N-3)}$, while $\mathcal{E}_3(\lambda) \leqslant 2^{-2}$. When the nonlocal correlation extends over $N - 1$ qubits but not over the Nth, then $\mathcal{E}_N \leqslant \frac{1}{8}$. Similarly to the entanglement witness, values $\mathcal{E}_N \in]\frac{1}{8}, \frac{1}{4}]$ are accessible only to systems where the nonlocality encompasses all the qubits.

III. APPLICATION TO MANY-BODY PHYSICS

We now illustrate these general considerations with some prominent examples of spin-chain systems. In this context, the correlators of type $\mathcal{E}_m$ are known as formation probabilities

$$\mathcal{E}_m = |\langle \hat{\sigma}_\pm^{(1)} \otimes \hat{\sigma}_\pm^{(2)} \otimes \hat{\sigma}_\pm^{(3)} \cdots \otimes \hat{\sigma}_\pm^{(m)} \rangle|^2, \qquad (13)$$

where the expectation value is computed in a system consisting of N spins ($m \leqslant N$), for instance using a ground state of some Hamiltonian. Formation probabilities in spin chains have been studied for some time [38–41,70–75] with the focus on behavior of $\mathcal{E}_m$ in the thermodynamically large system. Here, instead we focus on finite systems and, even more importantly, we build upon the hierarchy introduced above to develop detailed "tomography" of the entanglement and nonlocality in the ground states of experimentally relevant Hamiltonians.

The choice of the signs in (13) that gives a maximal correlator $\mathcal{E}_m$ is motivated by the expected structure of correlations in the considered state. For instance, a GHZ state from Eq. (7) calls for a product of either rising or lowering operators. On the other hand, for a superposition of antiferromagnetic states,
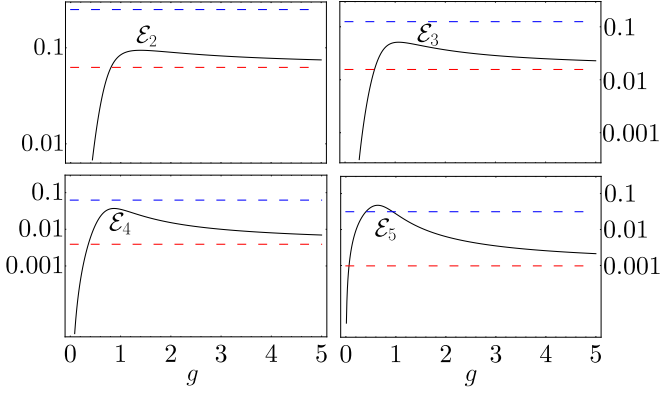
FIG. 1. Correlators $\mathcal{E}_m$ for $m \leqslant 5$ as a function of g calculated with the ground state of Hamiltonian (14) with $K = 0$ and $N = 6$. The horizontal dashed lines denote the entanglement bound 4^{-m} (lower, red) and the nonlocality bound 2^{-m} (upper, blue).

as considered in the next section, a product of alternating $\hat{\sigma}_+$ and $\hat{\sigma}_-$ is the correct one. Finally we remark that similar optimization issues arise in other Bell tests as well. For instance, orientation of the polarizers in the two-qubit Clauser-Horne-Shimony-Holt inequality should match the geometry of the state under consideration [76].

A. The Ising model with long-range interactions

We start with the Hamiltonian (with open boundary conditions)

$$\hat{H} = \sum_{j=1}^{N-1} \hat{\sigma}_z^{(j)} \hat{\sigma}_z^{(j+1)} + g \sum_{j=1}^{N} \hat{\sigma}_x^{(j)} + K \sum_{j=1}^{N-2} \hat{\sigma}_z^{(j)} \hat{\sigma}_z^{(j+2)}, \quad (14)$$

where the control parameter g is the magnitude of the external magnetic field in the x direction and K sets the strength of the long-range interactions. Note that all the Hamiltonians considered in this work are expressed in units of the nearest-neighbors energy, thus all the parameters, such as g and K, are dimensionless.

We first consider the $K = 0$ case, i.e., the Ising Hamiltonian in the antiferromagnetic phase. We solve the model numerically by the exact diagonalization of the Hamiltonian for $N = 6$. To detect the quantum properties in this antiferromagnetic phase, we adjust the correlator from (4) to

$$\mathcal{E}_m = |\langle \hat{\sigma}_+^{(1)} \otimes \hat{\sigma}_-^{(2)} \otimes \hat{\sigma}_+^{(3)} \cdots \otimes \hat{\sigma}_\pm^{(m)} \rangle|^2, \quad (15)$$

and consider five possibilities: $m \in [2, 6]$, namely, the correlators

$$\mathcal{E}_2 = |\langle \hat{\sigma}_+^{(1)} \otimes \hat{\sigma}_-^{(2)} \rangle|^2, \quad (16a)$$

$$\mathcal{E}_3 = |\langle \hat{\sigma}_+^{(1)} \otimes \hat{\sigma}_-^{(2)} \otimes \hat{\sigma}_+^{(3)} \rangle|^2, \quad (16b)$$

$$\mathcal{E}_4 = |\langle \hat{\sigma}_+^{(1)} \otimes \hat{\sigma}_-^{(2)} \otimes \hat{\sigma}_+^{(3)} \otimes \hat{\sigma}_-^{(4)} \rangle|^2, \quad (16c)$$

$$\mathcal{E}_5 = |\langle \hat{\sigma}_+^{(1)} \otimes \hat{\sigma}_-^{(2)} \otimes \hat{\sigma}_+^{(3)} \otimes \hat{\sigma}_-^{(4)} \otimes \hat{\sigma}_+^{(5)} \rangle|^2, \quad (16d)$$

$$\mathcal{E}_6 = |\langle \hat{\sigma}_+^{(1)} \otimes \hat{\sigma}_-^{(2)} \otimes \hat{\sigma}_+^{(3)} \otimes \hat{\sigma}_-^{(4)} \otimes \hat{\sigma}_+^{(5)} \otimes \hat{\sigma}_-^{(6)} \rangle|^2. \quad (16e)$$

Figure 1 shows the first four correlators (16a)–(16d) as a function of $g \in [0, 5]$ with entanglement (4^{-m}) and nonlocality
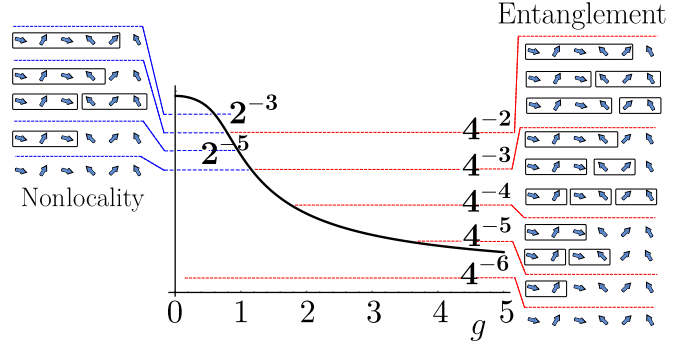

FIG. 2. The full six-spin correlator $\mathcal{E}_6$ (solid black line) calculated with the ground state of (14) as a function of g with $K = 0$ and $N = 6$. The horizontal red (entanglement, pointing to the right) and blue (nonlocality, pointing to the left) dashed lines separate regions, where $\mathcal{E}_6$ can be reproduced with a spin system with a specific multiparticle correlation (see the text for an explanation).

(2^{-m}) bounds marked. While the appearance of entanglement is witnessed by $\mathcal{E}_m$ starting from the lowest order $m = 2$, the Bell correlations are detected only at $m = 5$. All the correlators drop to zero as $g \to 0$. This is because for the vanishing magnetic field, the ground state is a superposition of two antiferromagnetic states

$$|\psi\rangle = \frac{1}{\sqrt{2}}(|\uparrow\downarrow\uparrow\downarrow\uparrow\downarrow\rangle + |\downarrow\uparrow\downarrow\uparrow\downarrow\uparrow\rangle). \quad (17)$$

Tracing out a single (say, the sixth) spin from such a maximally entangled state gives a classical mixture

$$\hat{\varrho} = \frac{1}{2}(|\psi_1\rangle\langle\psi_1| + |\psi_2\rangle\langle\psi_2|), \quad (18)$$

where $|\psi_1\rangle = |\uparrow\downarrow\uparrow\downarrow\uparrow\rangle$ and $|\psi_2\rangle = |\downarrow\uparrow\downarrow\uparrow\downarrow\rangle$. When $g \gg 1$, the ground state is that of the noninteracting spins, which explains why all the correlators drop as g grows and ultimately tend to 4^{-m}. We also observe that the Bell correlations are persistent around the critical point $g = 1$ of the quantum phase transition in quantum Ising chain. In the region of a phase transition the correlation length is large (approaching infinity in the thermodynamically large system). In such situation tracing out part of the system does not destroy the correlations within the subsystem what allows for $\mathcal{E}_m$ to stay large. This suggests the hierarchy of $\mathcal{E}_m$'s is an appropriate tool for exploring entanglement and nonlocality around the quantum phase transitions.

The $m = 6$ case, see Eq. (16d), is shown separately in Fig. 2. The $\mathcal{E}_6$ reaches its maximal value for $g = 0$ as it detects the quantum properties of the fully entangled state (17). We mark not only the entanglement- and the nonlocality-lower bound (4^{-6} and 2^{-6}) but also all the other limits derived from the considerations introduced in (8)–(12). This figure should be read as follows. When $\mathcal{E}_6 < 4^{-6}$, the correlation can be reproduced with a separable state of six spins [all six arrows on the right-hand side (RHS) of the plot unboxed]. When $\mathcal{E}_6 \in]4^{-6}, 4^{-5}[$, the correlation can be reproduced with a setup, where two spins are entangled and the other four form a separable state ($2 \times 1 \times 1 \times 1 \times 1$: two spins in a box, others unboxed). This is the most classical two-spin
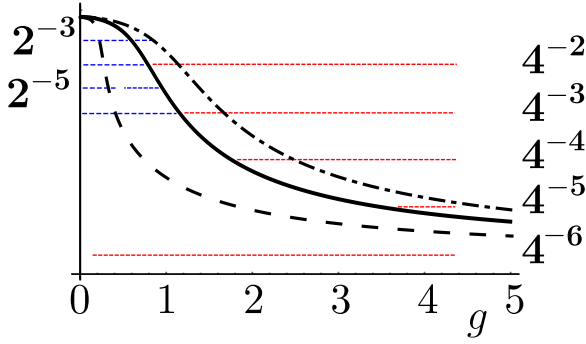
FIG. 3. The correlator $\mathcal{E}_6$ calculated with the Hamiltonian (14) for $K = 0$ (solid black line), $K = 0.4$ (dashed), and $K = -0.4$ (dot-dashed). The horizontal lines separate regions of multiqubit entanglement and nonlocality in the same fashion as in Fig. 2.

entangled state. Higher two-spin entangled states can be used to explain the correlation strength in the range $\mathcal{E}_6 \in]4^{-5}, 4^{-4}[$ ($2 \times 2 \times 1 \times 1$) or $\mathcal{E}_6 \in]4^{-4}, 4^{-3}[$ ($2 \times 2 \times 2$). All other cases are visually shown on the RHS of Fig. 2. Similarly, when $\mathcal{E}_6 < 2^{-6}$, the correlator can be modeled with a full LHV theory. When $\mathcal{E}_6 \in]2^{-6}, 2^{-5}[$, at least two spins are nonlocally correlated, and so forth.

We now test the impact of longer-range interactions on the quantum correlations [$K \neq 0$ in (14)]. We expect that turning on ferromagnetic ($K < 0$) interaction should strengthen the entanglement in the ordered ($g < 1$) phase and weaken it if the interaction is antiferromagnetic ($K > 0$) and competes with the nearest-neighbor interaction. Figure 3 compares the $\mathcal{E}_6$ for $K = 0$ and $K = \pm 0.4$ and confirms these expectations. Turning on the K parameter allows us also to study more deeply the relation between the hierarchy of the correlations and the quantum phase transition. The position of the critical point, for the competing interaction ($K > 0$), was studied before [77–79] with the conclusion that for intermediate values of $K < 0.5$ the critical point is given by $g_c = 1 - 2K$. From Fig. 1 we observe that for the system size $N = 6$, the correlator $\mathcal{E}_3$ has a maximal value close to the critical point $g_c = 1$ of a short-range Ising model. Guided by this observation we perform the finite-size scaling of the position of the maximum of $\mathcal{E}_{N/2}$, always in the form of

$$\mathcal{E}_{N/2} = |\langle \hat{\sigma}_+^{(1)} \otimes \hat{\sigma}_-^{(2)} \otimes \cdots \otimes \hat{\sigma}_+^{(N/2-1)} \otimes \hat{\sigma}_-^{(N/2)} \rangle|^2, \quad (19)$$

for chains of length $N = 8, 12, 16, 20$ and for different values of K. The results are presented in Fig. 4 and show that maximum of $\mathcal{E}_{N/2}$ coincides with the position of the phase transition. We note, however, that $\mathcal{E}_{N/2}$ does not seem to exhibit a singularity at the critical point and therefore is not a standard order parameter [1].

The results for the Ising models show how the hierarchy of correlations can be exploited to understand the quantum features of the many-body ground states extending from the detailed tomography of entanglement and nonlocality to the detection of quantum phase transitions.
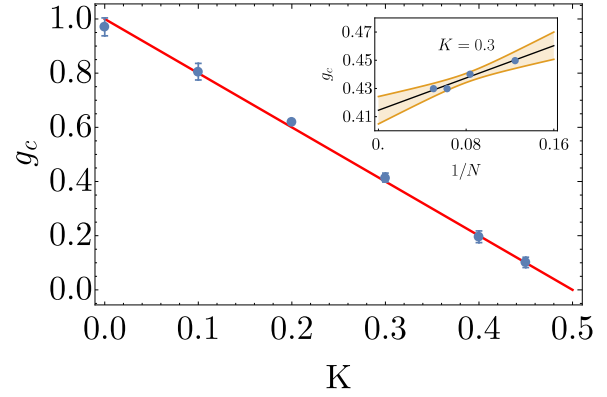

FIG. 4. Blue dots are the results of finite-size scaling of the position of the maximum of $\mathcal{E}_{N/2}$ using $N = 8, 12, 16, 20$ (the inset shows an example of scaling for $K = 0.3$). The solid red line denotes the quantum phase transition separating the antiferromagnetic phase from paramagnetic [77–79]. Error bars are from the linear fit estimation of the finite-size scaling. The shaded region in the inset represents the 0.9 confidence interval.

B. The XXZ quantum spin chains

We now focus on the XXZ spin-chain model [38,80] with the Hamiltonian

$$\hat{H} = \sum_{j=1}^{N} \left(\hat{\sigma}_x^{(j)} \hat{\sigma}_x^{(j+1)} + \hat{\sigma}_y^{(j)} \hat{\sigma}_y^{(j+1)} + \Delta \hat{\sigma}_z^{(j)} \hat{\sigma}_z^{(j+1)} \right), \quad (20)$$

where Δ is the anisotropy parameter and we assume the periodic boundary conditions. We will explore the effect of the finite temperature on the hierarchy and show that the correlations are naturally expressible in the language of the Bethe ansatz solution. The XXZ Hamiltonian exhibits quantum phase transitions at $\Delta = \pm 1$ separating a ferromagnetic phase ($\Delta < -1$) from paramagnetic ($|\Delta| < 1$) and antiferromagnetic ($\Delta > 1$). We focus on the regime with $\Delta > -1$. For the chain of length $N = 4$ the correlator $\mathcal{E}_4$,

$$\mathcal{E}_4 = |\langle \hat{\sigma}_+^{(1)} \otimes \hat{\sigma}_-^{(2)} \otimes \hat{\sigma}_+^{(3)} \otimes \hat{\sigma}_-^{(4)} \rangle|^2, \quad (21)$$

can be computed explicitly even at finite temperature (see Appendix A) with the result

$$\mathcal{E}_4 = \frac{1}{\mathcal{Z}^2} \left[-\frac{e^{-\beta(\Delta + \sqrt{8 + \Delta^2})}}{2} + \frac{1}{4}\left(1 + \frac{\Delta}{\sqrt{8 + \Delta^2}}\right) \right.$$
$$\left. + \frac{1}{4}\left(1 - \frac{\Delta}{\sqrt{8 + \Delta^2}}\right) e^{-2\beta\sqrt{8 + \Delta^2}} \right]^2, \quad (22)$$

$$\mathcal{Z} = 1 + e^{-\beta(E_+ - E_-)} + e^{-\beta(-\Delta - E_-)} + 2e^{-\beta(-1 - E_-)}$$
$$+ 7e^{\beta E_-} + 2e^{-\beta(1 - E_-)} + 2e^{-\beta(\Delta - E_-)}. \quad (23)$$

This result is plotted in Fig. 5 for four values of β as a function of Δ. Since Δ sets the energy scale in this problem, we expect the Bell correlation to vanish for $\beta \lesssim \Delta$, as confirmed in the plot. Interestingly, even for quite large $\beta = 2$, the correlation still cannot be modeled with a two-particle entangled state
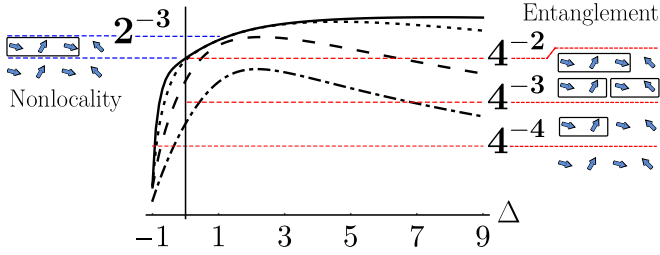
FIG. 5. $\mathcal{E}_4$ from (22) as a function of Δ for $\beta = 10$ (solid), $\beta = 5$ (dotted), $\beta = 2$ (dashed), and $\beta = 1$ (dot-dashed). The horizontal lines separate regions of multiqubit entanglement and nonlocality, as in Fig. 2, but calculated for $N = 4$.

around $\Delta = 1$. In the limit of $T \to 0$ we obtain

$$\mathcal{E}_4 = \frac{1}{16}\left(1 + \frac{\Delta}{\sqrt{8 + \Delta^2}}\right)^2. \tag{24}$$

This is bigger than the LHV limit 2^{-4} iff $\Delta > 0$. It also crosses other entanglement and nonlocality limits. For instance, when $\Delta > 2\sqrt{\sqrt{2} - 1}$, then $\mathcal{E}_4 > 2^{-3}$, which means that the correlator can be reproduced only with a four-spin entangled system where also all four spins are nonlocally correlated. These results show that the hierarchy provides insights into quantum-mechanical features of many-body systems also at finite temperatures.

Bethe ansatz solution

The *XXZ* spin chain of an arbitrary length can be exactly solved with the Bethe ansatz technique giving a direct access to the correlator $\mathcal{E}_N$ in the ground state

$$\mathcal{E}_N = |\langle \hat{\sigma}_+^{(1)} \otimes \hat{\sigma}_-^{(2)} \otimes \hat{\sigma}_+^{(3)} \cdots \rangle|^2$$
$$= |\langle GS|\downarrow\uparrow\downarrow \ldots\rangle|^2 |\langle \uparrow\downarrow\uparrow \ldots |GS\rangle|^2. \tag{25}$$

The overlaps $\langle GS|\downarrow\uparrow\downarrow \ldots\rangle$ and $\langle \uparrow\downarrow\uparrow \ldots |GS\rangle$ are known exactly for arbitrary N and Δ (for details, see Appendix A). Lower-order correlators are also accessible. Figure 6 shows the results for $N = 10$, together with the outcome of the numerical diagonalization of the Hamiltonian (20). In the analysis of the results we focus on two isotropic points $\Delta = \pm 1$ noting that the correlators are much larger for the former. This can be traced back to the structure of their ground states. Namely, for the $\Delta = 1$ the ground state is best understood as an entangled state of many magnons, whereas for $\Delta = -1$ it corresponds to a structureless vacuum [80].

C. Majumdar-Ghosh model

Finally, we consider the Majumdar-Ghosh model [55,56] with periodic boundary conditions, depicted by the Hamiltonian

$$\hat{H} = \sum_{\{j\}} \hat{\vec{\sigma}}^{(j)} \hat{\vec{\sigma}}^{(j+1)} + \frac{1}{2} \sum_{\{j\}} \hat{\vec{\sigma}}^{(j)} \hat{\vec{\sigma}}^{(j+2)}. \tag{26}$$

Its (translationally invariant) ground state

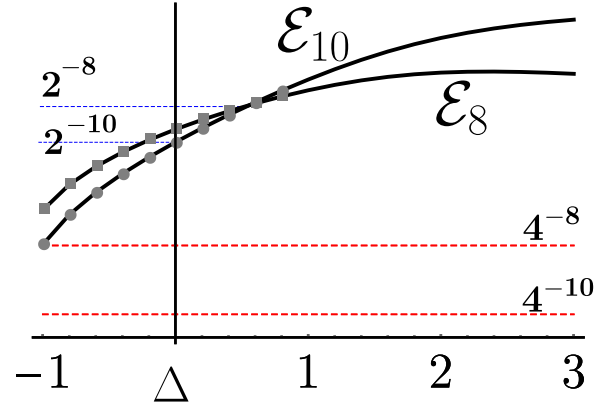$$|\psi\rangle = \mathcal{N}^{-1}(|\psi_1\rangle + |\psi_2\rangle) \tag{27}$$

FIG. 6. The ground-state correlators $\mathcal{E}_{10}$ and $\mathcal{E}_8$ for the *XXZ* spin chain of length $N = 10$ as a function of the anisotropy Δ (solid black lines). We show the analytic results (gray points) of Bethe ansatz (25) and the results of numerical diagonalization (black solid line) of the *XXZ* Hamiltonian (20). In the $\Delta \to \infty$ the correlators approach those of the Ising model with $g = 0$. The horizontal lines denote the lower bounds for 8- and 10-qubit entanglement (4^{-8} and 4^{-10}) and nonlocality (2^{-8} and 2^{-10}).

is a superposition of two products of singlet states

$$|\psi_1\rangle = \bigotimes_{j=0}^{(N/2)-1} \frac{|\uparrow_{2j+1}, \downarrow_{2j+2}\rangle - |\downarrow_{2j+1}, \uparrow_{2j+2}\rangle}{\sqrt{2}}, \tag{28}$$

$$|\psi_2\rangle = \bigotimes_{j=0}^{(N/2)-1} \frac{|\uparrow_{2j+2}, \downarrow_{2j+3}\rangle - |\downarrow_{2j+2}, \uparrow_{2j+3}\rangle}{\sqrt{2}}. \tag{29}$$

Here, $\mathcal{N}$ stands for the normalization. The explicit construction of the ground state for arbitrary N allows for analytic computations of the antiferromagnetic correlator, as in (15). For $N/2$ even we obtain, using the antiferromagnetic correlator as in Eq. (15),

$$\mathcal{E}_N = \frac{1}{(1 + 2^{N/2-1})^2}, \tag{30}$$

which brakes the Bell limit 2^{-N} (and therefore also the entanglement limit 2^{-2N}). For details, see Appendix B. The lower-order correlations are also accessible. For $\mathcal{E}_{N-2}$ we find

$$\mathcal{E}_{N-2} = \frac{1}{4}\mathcal{E}_N. \tag{31}$$

We observe that breaking the Bell limit is solely because the ground state is the superposition of $|\psi_1\rangle$ and $|\psi_2\rangle$ states. Indeed, the $\mathcal{E}_m$ correlator on $|\psi_1\rangle$ is equal to 2^{-m} and it is the admixture of $|\psi_2\rangle$ that lifts it above the threshold. Thus the ground state of the Majumdar-Ghosh model is a simple example of a state for which the hierarchy of the correlators breaks the Bell limit.

IV. CONCLUSIONS AND OUTLOOK

We have demonstrated that the multiparticle entanglement and the Bell nonlocality in many-body systems of qubits can be traced back to a single element of the density matrix. We have shown that the value of this element contains information about the number of entangled and Bell-correlated qubits. This allows one to track how the quantum features

expand over a large distance and number of particles, for instance in spin chains. This method could be used to tailor and witness highly nonclassical effects in many-body systems with possible applications to quantum computing, ultraprecise metrology, or large-scale tests of quantum mechanics. Furthermore, the observable, formation probability, is accessible experimentally with the current state-of-the-art in the field of quantum simulators. Moreover, a preliminary investigation of some experimentally reconstructed density matrices suggests that detailed information about quantum correlations can be extracted from the existing data [81–83].

We have also shown that the lower-order correlators detect a quantum phase transition: the critical value being correlated with the maxima of the correlators. Whether an honest order parameter exhibiting singularity at the phase transition can be constructed from $\mathcal{E}_m$ is an interesting open problem.

The results of our work create a new incentive to study formation probabilities and further extend existing techniques of their computations in the Bethe ansatz models. Another interesting problem is the computation, with the techniques of the asymptotic expansion [41,71], of the thermodynamic limit of $\mathcal{E}_{N/2}$, given its relation to the quantum phase transition.

ACKNOWLEDGMENTS

APPENDIX A: CORRELATIONS IN THE *XXZ* SPIN CHAIN

In this Appendix we show the computation of correlator $\mathcal{E}_m$ for the *XXZ* Hamiltonian

$$\hat{H} = \sum_{j=1}^{N} \left(\hat{\sigma}_x^{(j)} \hat{\sigma}_x^{(j+1)} + \hat{\sigma}_y^{(j)} \hat{\sigma}_y^{(j+1)} + \Delta \hat{\sigma}_z^{(j)} \hat{\sigma}_z^{(j+1)} \right). \quad \text{(A1)}$$

This Hamiltonian is exactly solvable by the Bethe ansatz methods for any N [38,80]. For a short chain of length $N = 4$ the eigenproblem can be solved by a direct diagonalization of the Hamiltonian, e.g., see [84]. We start with this special case as it allows one to easily include thermal effects, and turn to the Bethe ansatz solution afterwards.

1. Four-spins chain

The thermal density matrix is

$$\hat{\varrho}_T = \frac{1}{\mathcal{Z}} \sum_n e^{-\beta E_n} |\psi^{(n)}\rangle\langle\psi^{(n)}|, \quad \text{(A2)}$$

where the summation runs through all the eigenlevels $(\hat{H}|\psi^{(n)}\rangle = E_n|\psi^{(n)}\rangle)$ of the four-spin Hamiltonian from (20) and $\beta = (k_B T)^{-1}$ (T is the temperature, k_B the Boltzmann

constant, and $\mathcal{Z}$ is the statistical sum). The spectrum consists of 16 states out of which 3 have nonzero expectation values

$$|\langle E_\pm|\hat{\sigma}_+^{(1)} \hat{\sigma}_-^{(2)} \hat{\sigma}_+^{(3)} \hat{\sigma}_-^{(4)}|E_\pm\rangle| = \frac{1}{4} \left| 1 \mp \frac{\Delta}{\sqrt{8 + \Delta^2}} \right|, \quad \text{(A3)}$$

$$|\langle E_\Delta|\hat{\sigma}_+^{(1)} \hat{\sigma}_-^{(2)} \hat{\sigma}_+^{(3)} \hat{\sigma}_-^{(4)}|E_\Delta\rangle| = \frac{1}{2}, \quad \text{(A4)}$$

where $\hat{H}|E_\pm\rangle = E_\pm|E_\pm\rangle$ and $\hat{H}|E_\Delta\rangle = -\Delta|E_\Delta\rangle$ with

$$E_\pm = \frac{1}{2}(-\Delta \pm \sqrt{8 + \Delta^2}), \quad \text{(A5)}$$

and $|E_-\rangle$ being the ground state for $\Delta > -1$. In the local spin basis these states are

$$|E_\pm\rangle = \mathcal{N}_\pm \left(\frac{\Delta \pm \sqrt{8 + \Delta^2}}{2\sqrt{2}} |AF_2\rangle + |AF\rangle \right), \quad \text{(A6)}$$

$$|E_\Delta\rangle = \frac{1}{\sqrt{2}}(|\uparrow\downarrow\uparrow\downarrow\rangle - |\downarrow\uparrow\downarrow\uparrow\rangle), \quad \text{(A7)}$$

with

$$|AF_2\rangle = \frac{1}{2}(|\uparrow\uparrow\downarrow\downarrow\rangle + |\downarrow\uparrow\uparrow\downarrow\rangle + |\downarrow\downarrow\uparrow\uparrow\rangle + |\uparrow\downarrow\downarrow\uparrow\rangle), \quad \text{(A8)}$$

$$|AF\rangle = \frac{1}{\sqrt{2}}(|\uparrow\downarrow\uparrow\downarrow\rangle + |\downarrow\uparrow\downarrow\uparrow\rangle), \quad \text{(A9)}$$

and $\mathcal{N}_\pm$ appropriate normalization factors. The correlator reads

$$\mathcal{E}_4 = \frac{1}{\mathcal{Z}^2} \left[-\frac{e^{-\beta(\Delta + \sqrt{8+\Delta^2})}}{2} + \frac{1}{4} \left(1 + \frac{\Delta}{\sqrt{8 + \Delta^2}} \right) \right.$$

$$\left. + \frac{1}{4} \left(1 - \frac{\Delta}{\sqrt{8 + \Delta^2}} \right) e^{-2\beta\sqrt{8+\Delta^2}} \right]^2, \quad \text{(A10)}$$

$$\mathcal{Z} = 1 + e^{-\beta(E_+ - E_-)} + e^{-\beta(-\Delta - E_-)} + 2e^{-\beta(-1 - E_-)}$$

$$+ 7e^{\beta E_-} + 2e^{-\beta(1 - E_-)} + 2e^{-\beta(\Delta - E_-)}, \quad \text{(A11)}$$

for the antiferromagnetic product of four rising and lowering operators as in (15).

2. Bethe ansatz solution

Bethe ansatz provides the exact eigenstates of the system expressed as a superposition of states in the local spin basis [38,80]

$$|\Psi_M(\lambda_M)\rangle = \frac{1}{M!} \sum_{m_1,\dots,m_M=1}^{N} \chi(\mathbf{m}_M|\lambda_M)|\mathbf{m}_M\rangle, \quad \text{(A12)}$$

where

$$|\mathbf{m}_M\rangle = \hat{\sigma}_-^{(m_1)} \cdots \hat{\sigma}_-^{(m_M)}|0\rangle_+, \quad \text{(A13)}$$

and $|0\rangle_+$ is the fully polarized state with all the spins up. Here the bold symbol denotes set, $\lambda_M = \{\lambda_j\}_{j=1}^{M}$. The amplitude $\chi(\mathbf{m}_M|\lambda_M)$ is determined by the Bethe ansatz methods and is parametrized by the rapidities λ_M solving the Bethe equations

$$\theta_1(\lambda_j) = \frac{2\pi I_j}{N} - \frac{1}{N} \sum_{k=1}^{M} \theta_2(\lambda_j - \lambda_k), \qquad j = 1, \dots, M, \quad \text{(A14)}$$

The momentum and two-body scattering phase shift in the gapless phase ($|\Delta < 1|$) are

$$p(\lambda) = i\ln\frac{\cosh(\lambda - i\eta)}{\cosh(\lambda + i\eta)}, \tag{A15}$$

$$\theta(\lambda) = i\ln\frac{\sinh(2i\eta + \lambda)}{\sinh(2i\eta - \lambda)}. \tag{A16}$$

The quantum numbers I_j in (A14) for a ground state $|\mathrm{GS}\rangle$ (in the zero external magnetic field) are $I_j^{\mathrm{GS}} = -\frac{M+1}{2} + j$ for $j = 1, \ldots, M$ with $M = N/2$. The amplitudes are

$$\chi(\mathbf{m}_M|\lambda_M) = \frac{1}{|\mathcal{N}_M|}\sum_{\sigma \in \mathcal{P}_M}(-1)^{|\sigma|}\exp\left(-i\sum_{j=1}^{M}m_j p(\lambda_{\sigma_j})\right)$$

$$\times \exp\left(-\frac{i}{2}\sum_{k>j}\theta(\lambda_{\sigma_k} - \lambda_{\sigma_j})\right). \tag{A17}$$

where the normalization $\mathcal{N}_M$ is

$$|\mathcal{N}_M|^2 = \frac{\det G_M}{\prod_{j=1}^{M}K_1(\lambda_j)}, \tag{A18}$$

and guarantees that $\langle\Psi_M|\Psi_M\rangle = 1$. The factors appearing in the normalization are the Gaudin matrix

$$G_{jk} = \delta_{jk}\left(NK_1(\theta_j) - \sum_{m=1}^{M}K_2(\lambda_j - \lambda_m)\right) + K_2(\lambda_j - \lambda_k) \tag{A19}$$

and functions

$$K_1(\lambda) = \frac{\sin 2\eta}{\cosh(\lambda - i\eta)\cosh(\lambda + i\eta)}, \tag{A20}$$

$$K_2(\lambda) = \frac{\sin 4\eta}{\sinh(\lambda - 2i\eta)\sinh(\lambda + 2i\eta)}. \tag{A21}$$

The representation of the wave function in the Bethe ansatz solvable systems is specifically convenient for computation of the correlation functions $\mathcal{E}_m$. In the ground state the maximal correlator

$$\mathcal{E}_N = |\langle\mathrm{GS}|\downarrow\uparrow\downarrow\ldots\rangle|^2|\langle\uparrow\downarrow\uparrow\ldots|\mathrm{GS}\rangle|^2 \tag{A22}$$

and the overlaps $\langle\mathrm{GS}|\downarrow\uparrow\downarrow\ldots\rangle$ and $\langle\uparrow\downarrow\uparrow\ldots|\mathrm{GS}\rangle$ are given directly by the corresponding component of the ground-state wave function (A12)

$$\langle\mathrm{GS}|\downarrow\uparrow\downarrow\ldots\rangle = \chi(\mathrm{O_N}|\lambda_M), \tag{A23}$$

$$\langle\uparrow\downarrow\uparrow\ldots|\mathrm{GS}\rangle = \chi(\mathrm{E_N}|\lambda_N). \tag{A24}$$

Here $E_m = \{2, 4, \ldots, m\}$ and $O_m = \{1, 3, \ldots, m-1\}$. Lower-order correlation functions are also directly expressible in terms of the amplitudes $\chi(\mathbf{m}_M|\lambda_M)$. For example,

$$\mathcal{E}_{N-2} = |\chi^*(O_{N-2}, N|\lambda_M)\chi(E_{N-2}, N|\lambda_M)$$

$$+ \chi^*(O_{N-2}, N-1|\lambda_M)\chi(E_{N-2}, N-1|\lambda_M)|^2. \tag{A25}$$

APPENDIX B: CORRELATIONS IN THE MAJUMDAR-GHOSH MODEL

The explicit construction of the ground state of the Majumdar-Ghosh for arbitrary N [see Eq. (27)] allows for analytic computations of the antiferromagnetic correlator

$$\hat{\mathcal{A}}_N = \hat{\sigma}_+^{(1)}\hat{\sigma}_-^{(2)}\cdots\hat{\sigma}_+^{(N-1)}\hat{\sigma}_-^{(N)}. \tag{B1}$$

This gives

$$\langle\psi_{1,2}|\hat{\mathcal{A}}_N|\psi_{1,2}\rangle = \left(-\tfrac{1}{2}\right)^{N/2}, \tag{B2}$$

$$\langle\psi_{2,1}|\hat{\mathcal{A}}_N|\psi_{1,2}\rangle = \left(\tfrac{1}{2}\right)^{N/2}, \tag{B3}$$

which leads to the correlator

$$\langle\psi|\hat{\mathcal{A}}_N|\psi\rangle = \frac{1 + (-1)^{N/2}}{2}\frac{1}{1 + 2^{N/2-1}}, \tag{B4}$$

yielding, for $N/2$ even,

$$\mathcal{E}_N = \frac{1}{(1 + 2^{N/2-1})^2}, \tag{B5}$$

which breaks the Bell limit 2^{-N} (and therefore also the entanglement limit 2^{-2N}).

We also compute $\mathcal{E}_{N-2}$ (as $\mathcal{E}_{N-1} = 0$). To this end we observe that

$$\langle\psi_1|\hat{\mathcal{A}}_{N-2}|\psi_1\rangle = \left(-\tfrac{1}{2}\right)^{N/2-1}, \tag{B6}$$

$$\langle\psi_2|\hat{\mathcal{A}}_{N-2}|\psi_1\rangle = -\left(\tfrac{1}{2}\right)^{N/2}, \tag{B7}$$

$$\langle\psi_2|\hat{\mathcal{A}}_{N-2}|\psi_2\rangle = 0. \tag{B8}$$

Therefore

$$\langle\psi|\hat{\mathcal{A}}_{N-2}|\psi\rangle = -\frac{1}{2}\frac{1}{1 + 2^{N/2-1}}, \tag{B9}$$

and we obtain

$$\mathcal{E}_{N-2} = \tfrac{1}{4}\mathcal{E}_N. \tag{B10}$$

[1] S. Sachdev, *Quantum Phase Transitions* (Cambridge University Press, Cambridge, UK, 1999).

[2] V. Giovannetti, S. Lloyd, and L. Maccone, Science **306**, 1330 (2004).

[3] J. Tura, R. Augusiak, A. B. Sainz, T. Vértesi, M. Lewenstein, and A. Acín, Science **344**, 1256 (2014).

[4] L. Pezzè, A. Smerzi, M. K. Oberthaler, R. Schmied, and P. Treutlein, Rev. Mod. Phys. **90**, 035005 (2018).

[5] C. Monroe, Nature (London) **416**, 238 (2002).

[6] B. Zeng, X. Chen, D.-L. Zhou, and X.-G. Wen, *Quantum Information Meets Quantum Matter* (Springer, New York, 2019).

[7] I. M. Georgescu, S. Ashhab, and F. Nori, Rev. Mod. Phys. **86**, 153 (2014).

[8] J. Esteve, C. Gross, A. Weller, S. Giovanazzi, and M. Oberthaler, Nature (London) **455**, 1216 (2008).

[9] M. F. Riedel, P. Böhi, Y. Li, T. W. Hänsch, A. Sinatra, and P. Treutlein, Nature (London) **464**, 1170 (2010).

[10] C. Gross, T. Zibold, E. Nicklas, J. Esteve, and M. K. Oberthaler, Nature (London) **464**, 1165 (2010).

[11] I. D. Leroux, M. H. Schleier-Smith, and V. Vuletić, Phys. Rev. Lett. **104**, 250801 (2010).

[12] H. Strobel, W. Muessel, D. Linnemann, T. Zibold, D. B. Hume, L. Pezzé, A. Smerzi, and M. K. Oberthaler, Science **345**, 424 (2014).

[13] I. Bloch, J. Dalibard, and S. Nascimbène, Nat. Phys. **8**, 267 (2012).

[14] W. Hofstetter and T. Qin, J. Phys. B: At., Mol. Opt. Phys. **51**, 082001 (2018).

[15] A. Browaeys and T. Lahaye, Nat. Phys. **16**, 132 (2020).

[16] F. Schmidt-Kaler, H. Häffner, M. Riebe, S. Gulde, G. P. Lancaster, T. Deuschle, C. Becher, C. F. Roos, J. Eschner, and R. Blatt, Nature (London) **422**, 408 (2003).

[17] T. R. Tan, J. P. Gaebler, Y. Lin, Y. Wan, R. Bowler, D. Leibfried, and D. J. Wineland, Nature (London) **528**, 380 (2015).

[18] H. Häffner, W. Hänsel, C. Roos, J. Benhelm, M. Chwalla, T. Körber, U. Rapol, M. Riebe, P. Schmidt, C. Becher *et al.*, Nature (London) **438**, 643 (2005).

[19] R. Blatt and D. Wineland, Nature (London) **453**, 1008 (2008).

[20] S. Korenblit, D. Kafri, W. C. Campbell, R. Islam, E. E. Edwards, Z.-X. Gong, G.-D. Lin, L.-M. Duan, J. Kim, K. Kim, and C. Monroe, New J. Phys. **14**, 095024 (2012).

[21] R. Blatt and C. F. Roos, Nat. Phys. **8**, 277 (2012).

[22] J. G. Bohnet, B. C. Sawyer, J. W. Britton, M. L. Wall, A. M. Rey, M. Foss-Feig, and J. J. Bollinger, Science **352**, 1297 (2016).

[23] A. A. Houck, H. E. Türeci, and J. Koch, Nat. Phys. **8**, 292 (2012).

[24] A. D. Córcoles, E. Magesan, S. J. Srinivasan, A. W. Cross, M. Steffen, J. M. Gambetta, and J. M. Chow, Nat. Commun. **6**, 6979 (2015).

[25] J. Plantenberg, P. De Groot, C. Harmans, and J. Mooij, Nature (London) **447**, 836 (2007).

[26] P. Calabrese and J. Cardy, J. Stat. Mech.: Theory Exp. (2004) P06002.

[27] M. B. Hastings, J. Stat. Mech.: Theory Exp. (2007) P08024.

[28] F. Franchini, A. R. Its, and V. E. Korepin, J. Phys. A: Math. Theor. **41**, 025302 (2007).

[29] V. Alba, L. Tagliacozzo, and P. Calabrese, Phys. Rev. B **81**, 060411(R) (2010).

[30] V. Alba, M. Haque, and A. M. Läuchli, J. Stat. Mech.: Theory Exp. (2012) P08011.

[31] N. Laflorencie, Phys. Rep. **646**, 1 (2016).

[32] S. Wald, R. Arias, and V. Alba, J. Stat. Mech.: Theory Exp. (2020) 033105.

[33] K. Życzkowski, P. Horodecki, A. Sanpera, and M. Lewenstein, Phys. Rev. A **58**, 883 (1998).

[34] P. Calabrese, L. Tagliacozzo, and E. Tonni, J. Stat. Mech.: Theory Exp. (2013) P05002.

[35] P. Ruggiero, V. Alba, and P. Calabrese, Phys. Rev. B **94**, 035152 (2016).

[36] R. Islam, R. Ma, P. M. Preiss, M. Eric Tai, A. Lukin, M. Rispoli, and M. Greiner, Nature (London) **528**, 77 (2015).

[37] P. Hauke, M. Heyl, L. Tagliacozzo, and P. Zoller, Nat. Phys. **12**, 778 (2016).

[38] V. E. Korepin, N. M. Bogoliubov, and A. G. Izergin, *Quantum Inverse Scattering Method and Correlation Functions* (Cambridge University Press, Cambridge, 1993).

[39] M. Shiroishi, M. Takahashi, and Y. Nishiyama, J. Phys. Soc. Jpn. **70**, 3535 (2001).

[40] A. V. Razumov and Y. G. Stroganov, J. Phys. A: Math. Gen. **34**, 3185 (2001).

[41] A. G. Abanov and F. Franchini, Phys. Lett. A **316**, 342 (2003).

[42] R. Horodecki, P. Horodecki, M. Horodecki, and K. Horodecki, Rev. Mod. Phys. **81**, 865 (2009).

[43] A. Einstein, B. Podolsky, and N. Rosen, Phys. Rev. **47**, 777 (1935).

[44] J. S. Bell, Physics **1**, 195 (1964).

[45] N. Brunner, D. Cavalcanti, S. Pironio, V. Scarani, and S. Wehner, Rev. Mod. Phys. **86**, 419 (2014).

[46] E. G. Cavalcanti, C. J. Foster, M. D. Reid, and P. D. Drummond, Phys. Rev. Lett. **99**, 210405 (2007).

[47] Q. Y. He, P. D. Drummond, and M. D. Reid, Phys. Rev. A **83**, 032120 (2011).

[48] E. Cavalcanti, Q. Y. He, M. D. Reid, and H. M. Wiseman, Phys. Rev. A **84**, 032115 (2011).

[49] K. Kim, S. Korenblit, R. Islam, E. E. Edwards, M.-S. Chang, C. Noh, H. Carmichael, G.-D. Lin, L.-M. Duan, C. C. J. Wang, J. K. Freericks, and C. Monroe, New J. Phys. **13**, 105003 (2011).

[50] J. Simon, W. S. Bakr, R. Ma, M. E. Tai, P. M. Preiss, and M. Greiner, Nature (London) **472**, 307 (2011).

[51] H. Bernien, S. Schwartz, A. Keesling, H. Levine, A. Omran, H. Pichler, S. Choi, A. S. Zibrov, M. Endres, M. Greiner *et al.*, Nature (London) **551**, 579 (2017).

[52] S. de Léséleuc, S. Weber, V. Lienhard, D. Barredo, H. P. Büchler, T. Lahaye, and A. Browaeys, Phys. Rev. Lett. **120**, 113602 (2018).

[53] S. Murmann, F. Deuretzbacher, G. Zürn, J. Bjerlin, S. M. Reimann, L. Santos, T. Lompe, and S. Jochim, Phys. Rev. Lett. **115**, 215301 (2015).

[54] T. Graß and M. Lewenstein, EPJ Quantum Technol. **1**, 8 (2014).

[55] C. K. Majumdar and D. K. Ghosh, J. Math. Phys. **10**, 1388 (1969).

[56] C. K. Majumdar, J. Phys. C: Solid State Phys. **3**, 911 (1970).

[57] P. Hyllus, W. Laskowski, R. Krischek, C. Schwemmer, W. Wieczorek, H. Weinfurter, L. Pezzé, and A. Smerzi, Phys. Rev. A **85**, 022321 (2012).

[58] G. Tóth, Phys. Rev. A **85**, 022322 (2012).

[59] J. F. Sherson, C. Weitenberg, M. Endres, M. Cheneau, I. Bloch, and S. Kuhr, Nature (London) **467**, 68 (2010).

[60] R. Dall, A. Manning, S. Hodgman, W. RuGway, K. V. Kheruntsyan, and A. Truscott, Nat. Phys. **9**, 341 (2013).

[61] S. R. White, Phys. Rev. Lett. **69**, 2863 (1992).

[62] U. Schollwöck, Rev. Mod. Phys. **77**, 259 (2005).

[63] U. Schollwöck, Ann. Phys. **326**, 96 (2011).

[64] R. Orús, Nat. Rev. Phys. **1**, 538 (2019).

[65] R. Schmied, J.-D. Bancal, B. Allard, M. Fadel, V. Scarani, P. Treutlein, and N. Sangouard, Science **352**, 441 (2016).

[66] D. K. Shin, B. M. Henson, S. S. Hodgman, T. Wasak, J. Chwedeńczuk, and A. G. Truscott, Nat. Commun. **10**, 4447 (2019).

[67] J.-W. Pan, D. Bouwmeester, M. Daniell, H. Weinfurter, and A. Zeilinger, Nature (London) **403**, 515 (2000).

[68] D. Kielpinski, V. Meyer, C. A. Sackett, W. M. Itano, C. Monroe, and D. J. Wineland, Nature (London) **409**, 791 (2001).

[69] Q. Y. He, E. G. Cavalcanti, M. D. Reid, and P. D. Drummond, Phys. Rev. A **81**, 062106 (2010).

[70] A. G. Abanov, in *Applications of Random Matrices in Physics*, edited by É. Brézin, V. Kazakov, D. Serban, P. Wiegmann, and A. Zabrodin (Springer Netherlands, Dordrecht, 2006), pp. 139–161.

[71] A. G. Abanov, arXiv:cond-mat/0504307.

[72] J. Stolze and T. Garske, Condens. Matter Phys. **12**, 369 (2009).

[73] M. A. Rajabpour, Europhys. Lett. **112**, 66001 (2015).

[74] A. Morin-Duchesne, C. Hagendorf, and L. Cantini, J. Phys. A: Math. Theor. **85**, 022322 (2020).

[75] M. N. Najafi and M. A. Rajabpour, Phys. Rev. B **101**, 165415 (2020).

[76] J. F. Clauser, M. A. Horne, A. Shimony, and R. A. Holt, Phys. Rev. Lett. **23**, 880 (1969).

[77] M. Beccaria, M. Campostrini, and A. Feo, Phys. Rev. B **76**, 094410 (2007).

[78] A. K. Chandra and S. Dasgupta, Phys. Rev. E **75**, 021105 (2007).

[79] A. Nagy, New J. Phys. **13**, 023015 (2011).

[80] F. Franchini, *An Introduction to Integrable Techniques for One-Dimensional Quantum Systems*, Lecture Notes in Physics Vol. 940 (Springer, Cham, 2017), also available on arXiv:1609.02100.

[81] S. Filipp, P. Maurer, P. J. Leek, M. Baur, R. Bianchetti, J. M. Fink, M. Göppl, L. Steffen, J. M. Gambetta, A. Blais, and A. Wallraff, Phys. Rev. Lett. **102**, 200402 (2009).

[82] H. Mikami, Y. Li, K. Fukuoka, and T. Kobayashi, Phys. Rev. Lett. **95**, 150404 (2005).

[83] L. DiCarlo, M. D. Reed, L. Sun, B. R. Johnson, J. M. Chow, J. M. Gambetta, L. Frunzio, S. M. Girvin, M. H. Devoret, and R. J. Schoelkopf, Nature (London) **467**, 574 (2010).

[84] K. Kudo, Statistical and dynamical properties in the energy spectra of XXZ spin chains, Ph.D. thesis, Ochanomizu University, 2005.